The Damage Assessment for Rapid Response (DARR) Method and its Application to Different Ground-Motion Levels and Building Types

Bojana Petrovic[1] , Chiara Scaini[*1] , and Stefano Parolai[1,2]

Abstract

Seismic recordings in buildings and on the ground are increasingly available due to the increment and expansion of seismic monitoring networks worldwide. However, most urban strong-motion networks consist of stations installed at the ground or, less frequently, in selected building's basement. It is, therefore, of utmost importance to develop methods that can provide estimates of expected structural damage, starting from earthquake recordings at the ground level. Damage Assessment for Rapid Response (DARR) provides first-level estimates of the expected damage to buildings, based on ground-motion recordings and simple information on buildings' characteristics. In this work, we apply DARR using both weak and strong ground-motion recordings available for different low- and mid-rise building typologies. A total of 9 buildings and 19 earthquake recordings were analyzed. DARR reproduces the shaking at the building's top, and estimates the peak structural relative displacement or average interstory drift. Results show that the method works well for the considered building types and ground-motion levels for the estimation of relative and total displacements using first-order assessments. Comparison with the previously defined thresholds allows the estimation of expected damage. Our results (i.e., no damage for most buildings and events) are consistent with the absence of damaging events in northeastern Italy in the studied period (2019–2021). For a school building in central Italy, which was heavily damaged by the 2016 Central Italian sequence, DARR correctly predicted this fact.

Introduction

Seismic monitoring is a fundamental component of seismic risk reduction, because it allows the timely location of earthquakes and issues of seismic alerts (e.g., Wald, Wald, *et al.*, 2008; Espinosa-Aranda *et al.*, 2009). In the recent decades, the coverage of seismic monitoring has increased rapidly worldwide (e.g., Mori *et al.*, 1998; Okada *et al.*, 2004; Espinosa-Aranda *et al.*, 2009; Gorini *et al.*, 2010; Satriano *et al.*, 2011; Wu *et al.*, 2013; Parolai *et al.*, 2017). Earthquake recordings can be used to enrich rapid ground-motion estimates (e.g., using ShakeMaps, Wald *et al.*, 1999, 2006) that can support a first-level damage assessment shortly after earthquake occurrence (Wald, Earle, *et al.*, 2008). Unlike in standard seismic networks, cost-effective instruments are usually installed in the urban areas close to or in the buildings for building monitoring or earthquake early warning purposes (e.g., Clayton *et al.*, 2012; Wu *et al.*, 2013; Parolai *et al.*, 2017; Petrovic *et al.*, 2018; Bragato *et al.*, 2021).

Estimation of expected damage to buildings is paramount to support emergency managers in the aftermath of an earthquake. Damage to residential buildings are, in fact, responsible for a major fraction of casualties generated by a seismic event (So and Spence, 2013). Public buildings are often devoted to special functions during emergencies (e.g., gathering of civil protection volunteers, equipment, etc.) and are, therefore, of special interest for disaster response. Existing methods for damage assessment are mostly based on fragility curves, derived either empirically (e.g., Rota *et al.*, 2008; Masi *et al.*, 2019) or analytically (e.g., Borzi *et al.*, 2008; Donà *et al.*, 2020). Such curves associate a given ground-motion parameter

(e.g., peak ground acceleration [PGA]) with a damage level, but do not account for the frequency content of the ground motion. Most fragility curves are, in fact, defined without taking into account the experimental fundamental frequencies and thus the dynamic behavior of the different building typologies. Past events such as the 2016–2017 Central Italy sequence showed that events of magnitude between 5 and 6 can cause strong damage to the building stock, in particular, to masonry buildings (Fiorentino et al., 2018). However, there are very few damaged buildings in Italy for which mainshock earthquake recordings are available. Many recordings are available only at the ground level or in buildings damaged during aftershocks, with potential cumulative damage. One of the few notable examples is the Visso school, which was damaged by the first event of the Central Italy sequence and also suffered documented cumulative damage during the sequence (Graziotti et al., 2019; Brunelli et al., 2021).

For more than 80 years, seismic sensors have been used for monitoring specific buildings, in particular, in California (e.g., Trifunac et al., 2001; Ebrahimian et al., 2016). Recordings collected on buildings allow measuring the parameters associated with the dynamic behavior of a monitored building and identifying expected damage (Rahmani et al., 2015; Rahmani and Todorovska, 2021). Because of the recognized potential of seismic monitoring and the growing availability of low-cost sensors, the number of monitored buildings has been increasing in the recent decades. Traditional building monitoring provides a large number of reliable information on building dynamic response and allows structural health monitoring. Low-cost building monitoring requires the minimum of two sensors (at the top and the bottom of the building). Straser and Kiremidjian (1998) showed that buildings could be monitored by wireless low-cost sensors, reducing installation time and overall costs, enabling to monitor a large number of buildings. Bindi et al. (2016) provide an overview of the possible applications of low-cost seismic sensors for monitoring and assessing expected damage for single buildings. Strong-motion recordings on buildings allow to infer their expected dynamic response (Iervolino et al., 2016) and, subsequently, expected damage (Parolai et al., 2015). This is valid for the previously characterized buildings and building typologies for which information on the vibrational modes (e.g., from ambient vibration measurements) or period–height relations (e.g., Gallipoli et al., 2009) are available. Existing studies have shown that simplified models such as single-degree-of-freedom (SDOF) or multi-degree-of-freedom (MDOF) oscillators can successfully reproduce the building's linear dynamic response (e.g., Mucciarelli and Gallipoli, 2007). Parolai et al. (2015) validated the estimation of the acceleration at the top for two buildings: the first one modeled as an SDOF oscillator, and the second both as SDOF and MDOF oscillators. The first one is situated in L'Aquila (Picozzi et al., 2011) and the second one in Thessaloniki (Bindi et al., 2015). The method,

hereinafter referred to as Damage Assessment for Rapid Response (DARR), proposed by Scaini et al. (2021), was applied to estimate relative and total displacements at the top for a single building modeled as an SDOF oscillator for a small-magnitude event. Moreover, Scaini et al. (2021) showed the results of the application of DARR for buildings belonging to a specific typology (low-rise regular unreinforced masonry [URM]) assessing the expected damage for a simulated historical scenario. Peak structural relative displacement (PSRD, maximum displacement between top and bottom) can be used as a proxy to assess expected structural and nonstructural damage based on thresholds defined in the literature for different building typologies (e.g., Lagomarsino and Giovinazzi, 2006). Other authors provide interstory drift limits for structural damage occurrence in common typologies (e.g., Borzi et al., 2008; Rossetto et al., 2016).

In this study, we apply the DARR method for different ground motion levels and building types for which dynamic behavior is simulated using either SDOF or MDOF oscillators. We tested the performance of SDOF or MDOF oscillators for simulating the dynamic behavior of buildings of different construction type and height. As seismic inputs, we used earthquakes of different magnitudes, distances, and frequency contents, recorded by two seismological networks: Sistema di Monitoraggio terrestre dell'Italia Nord Orientale (SMINO, Bragato et al., 2021) and Osservatorio Sismico delle Strutture (OSS, Dolce et al., 2017). SMINO is a dense seismological network in northeastern Italy (Bragato et al., 2021) that includes an increasing number of low-cost sensors (currently 403) installed on about 350 selected buildings. The SMINO network has been only recently extended to installations also in buildings (which started in 2018). In the period 2019–2021, the events recorded in buildings are small-magnitude events or strong events occurred at distances over 200 km. OSS is the Italian national network of the Seismic Observatory of Structures, managed by the National Civil Protection (Dolce et al., 2017). In both the networks, sensors are installed at least at the bottom and top of the buildings. The vibrational frequencies and, thus, the estimation of the oscillator type is based on the previously collected ambient noise measurements or from the literature. The damping ratios are calculated with a best-fit method.

First, we briefly present the DARR method (Scaini et al., 2021). Then, we describe the studied buildings and the characterization of the input parameters, as well as the ground-motion recordings used for the analysis. The study is focused on nine low- and mid-rise masonry or reinforced concrete (RC) buildings for which we simulate the relative and total displacements generated by different events. The simulated peak structural relative displacements are compared with the observed ones (from the recordings). The procedure was performed for 19 building–earthquake pairs. The first event of the 2016 Central Italy sequence, an M_w 6.0 earthquake, is considered in the study. The other events have PGA mostly below

0.1 m/s² (small-magnitude events or large-magnitude events occurring at greater distances). Damage has been observed only after the 2016 Central Italy event; for all other events no damage has been reported. Based on relative displacement thresholds taken from the literature, we assessed the expected damage and compared the results with the empirical evidence. Finally, we discuss the results underlining their implications for rapid damage assessment purposes.

The DARR Method

The DARR method consists of three parts: (1) characterization of the input parameters, (2) the estimation of relative (drift) and total displacements at the top of a building, and (3) the damage assessment based on selected relative displacement (displacement between top and bottom) or interstory drift thresholds.

Characterization of the input parameters

The following parameters have to be defined for each building or building typology before a strong earthquake occurs. Once the parameters are defined, they will be used for all the subsequent events. Future studies and data may, of course, allow better tuning of parameters for a structure before the next earthquake.

Building typology (building height, construction material etc.). Buildings can be classified into typologies, defined based on their common characteristics (material, age, use). For example, historical URM constituted by stone blocks is very common in Europe. Building characteristics can be collected at multiple spatial scales, ranging from regional exposure models (e.g., Crowley *et al.*, 2020) to national and subnational datasets (e.g., building census). The main characteristics are usually the building material (and, in particular, the material of load-bearing structures), height, age and can be complemented with other construction details (e.g., roof type and footprint shape). Typologies are extremely useful for seismic risk assessment (Dolce *et al.*, 2021) and they allow to identify the expected behavior of buildings in case of earthquakes. The European Macroseismic Scale 1998 (EMS-98) scale (Grünthal, 1998), in particular, identifies building typologies representative for Europe, which are associated with vulnerability and fragility curves (Da Porto *et al.*, 2021). These studies led to the definition of limits (relative displacement and interstory drift thresholds) to be associated with building typologies, under the assumption that buildings belonging to the same typology have a similar dynamic response during earthquakes.

Vibration frequencies and oscillator type (SDOF or MDOF). For individual buildings, vibration frequencies are estimated from ambient vibration measurements at different locations in the building (at least one at the top and one at the bottom) using the spectral ratio method. If the fundamental mode makes the largest energy contribution, an SDOF oscillator is considered. Otherwise, the second vibration mode (weighted by their spectral amplitudes) is also used to define an MDOF oscillator. The vibration frequencies and the oscillator type are defined separately for the two main building directions. An SDOF oscillator may adequately simulate the dynamic behavior in one direction, whereas an MDOF oscillator may be required for the dynamic behavior of the other direction.

For building typologies, it is recommended to either use the vibration frequencies of a building representative of the building typology or estimate the fundamental frequency using period–height relationships from the literature (e.g., Gallipoli *et al.*, 2023) to define the SDOF oscillator. In this case, the same vibration frequency is assumed in both the directions.

Damping ratio. There are several methods for estimating the damping ratio for individual monitored buildings from ambient vibration (e.g., Mucciarelli and Gallipoli, 2007) or earthquake recordings (e.g., Snieder and Safak, 2006). However, there are very few studies on low-rise masonry buildings in the literature, so the estimation of the damping ratio using these methods may not be conclusive. In this case, the damping ratio can be estimated from a best-fit method using a recording of a small-magnitude earthquake.

For building typologies, either the damping ratio estimated for an individual building, which can be assumed to be representative of the entire building typology, or damping ratios from the literature (e.g., Eurocode 8, CEN, 2004) can be considered.

Damage thresholds. Interstory drift values associated with structural and nonstructural damage are provided by many building codes (e.g., Federal Emergency Management Agency [FEMA], 2012). However, the EC8 (CEN, 2004) only provides values for nonstructural damage. To correctly define the damage thresholds, information about the building typologies is needed. In fact, relative displacement (drift) or interstory drift limits are available for different building typologies and damage states (e.g., Ruiz-García and Negrete, 2009; Frankie *et al.*, 2013; Chourasia *et al.*, 2016). Each study analyzes the response of selected building typologies under specific assumptions, providing results that are valid for the typology and the study area. In particular, Lagomarsino and Giovinazzi (2006) estimated relative displacement limits for different damage levels (e.g., structural damage and collapse) and building typologies (Table 1) that belong to the EMS-98 classification (Grünthal, 1998). These studies led to the definition of limits (relative displacement and interstory drift thresholds) for different damage states to be associated with building typologies, under the assumption that buildings belonging to the same typology have a similar dynamic response during earthquakes. In particular, extensive damage corresponds to level-3 of EMS-98 (moderate structural damage and heavy nonstructural damage), and complete damage includes both level 4 and 5 of the EMS-98 scale (heavy and very heavy structural damage and/or collapse). Borzi *et al.* (2008) calculated interstory drift

Relative Displacement (in Centimeters) and Interstory Drift Limits (in Percentage) for Extensive and Complete Structural Damage for Selected Building Typologies (Simple Stone or Regular Unreinforced Masonry [URM], and Reinforced Concrete [RC] Frames and Shear Walls)

Building Typology	Relative Displacement (cm)		Interstory Drift Ratio (%)	
Damage Level	Extensive	Complete	Extensive	Complete
Simple stone URM, low-rise (1–2 stories)	0.85	1.40		
Simple stone URM, mid-rise (3–5 stories)	1.35	2.10		0.61
Simple stone URM, high-rise (>5 stories)	1.61	2.41	0.34	
Regular URM, RC floors, low-rise (1–2 stories)	1.38	2.36		
Regular URM, RC floors, mid-rise (3–5 stories)	2.19	3.50		0.45–0.72*
Regular URM, RC floors, high-rise (>5 stories)	2.47	3.87		
RC frame, low-rise (1–3 stories)	3.01	4.51	0.13	0.30
RC frame, mid-rise (4–7 stories)	4.49	6.74	0.12	0.27
RC frame, high-rise (>7 stories)	6.10	9.15	0.16	0.38
RC shear walls, low-rise (1–3 stories)	3.90	5.94	0.03	0.06
RC shear walls, mid-rise (4–7 stories)	6.12	9.59	0.12	0.28
RC shear walls, high-rise (>7 stories)	8.21	12.86	0.23	0.56

Relative displacement (displacement between top and bottom) limits are provided by Lagomarsino and Giovinazzi (2006). Interstory drift limits are provided by Borzi et al. (2008) for URM and by the deliverables of the Risk-UE project (Mouroux and Brun, 2006) for RC. Limits were calculated based on finite-element modeling of different building typologies and represent the threshold for occurrence of extensive and complete damage, corresponding to D3 and both D4 and D5 damage level of European Macroseismic Scale 1998 (EMS-98) (Grünthal, 1998). The same Interstory Drift Ratio limit is provided for all masonry buildings for extensive damage, whereas for complete damage one value is provided for stone and one for regular URM.
*Depending on percentage of voids.

limits for common masonry building types in Italy, while the deliverables of Risk-UE project (Mouroux and Brun, 2006) provide values for RC buildings (Table 1).
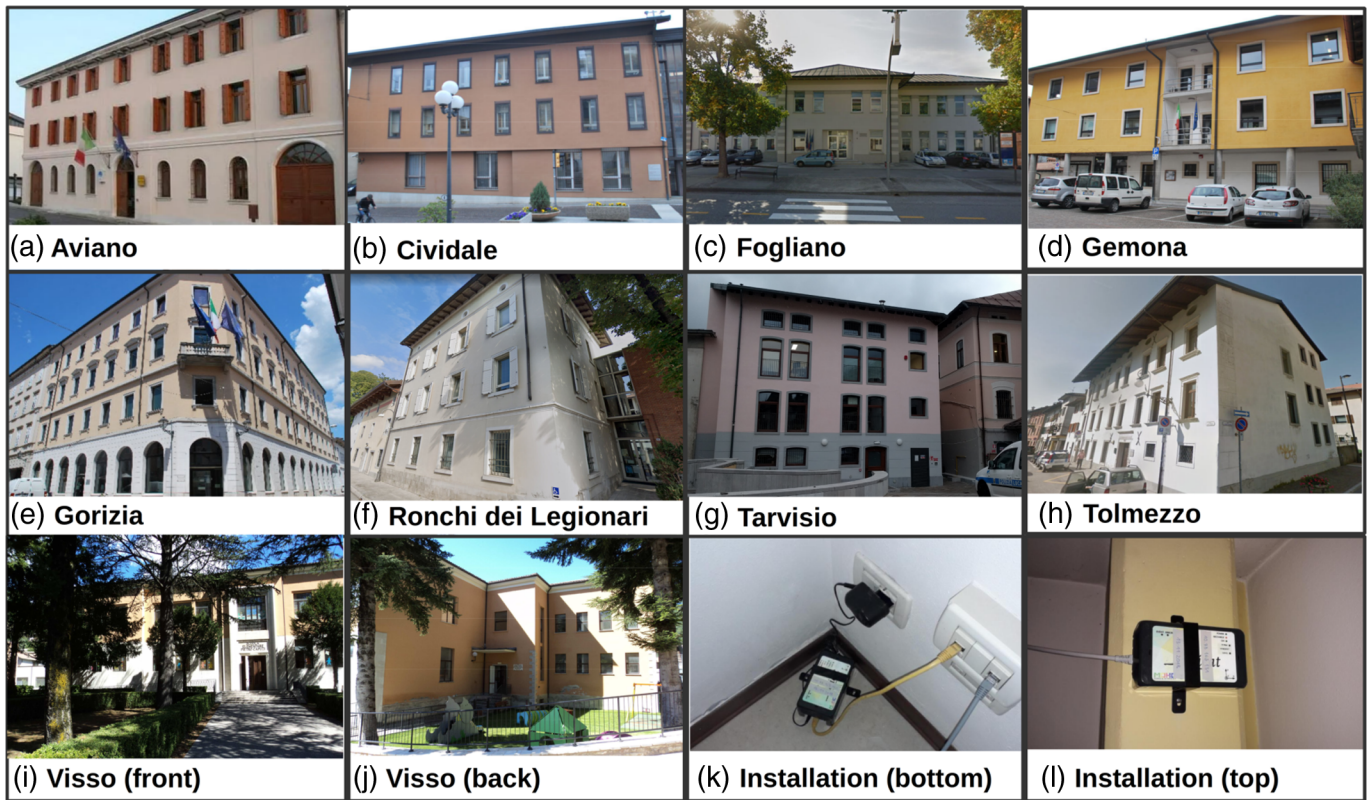
Estimation of relative and total displacements at the top

The estimation of relative and total displacements at the top of a building, based on the approach described in Parolai et al. (2015) and Scaini et al. (2021), is shortly summarized here. The building is assumed to behave in a first-order approximation as a damped linear SDOF or an MDOF oscillator, depending on the structure's dynamic response. The oscillator is characterized by the fundamental frequency or frequencies (weighted based on their spectral amplitudes) and the damping. The method requires, at least, a recording of an earthquake in the basement, on the ground floor or in the proximity of the considered building (where the soil conditions can be assumed as homogeneous). DARR is based on the Z-transform for the estimation of the relative acceleration, velocity, and displacement at the top of a building (e.g., Lee, 1990; Jin et al., 2004). Following Parolai et al. (2015), the total acceleration at the top of a building can be calculated as the sum of the acceleration at the basement or ground floor of the building and the relative acceleration estimated by the Z-transform (e.g., Lee, 1990; Jin et al., 2004) from this recording, modeling the building

by an SDOF or MDOF oscillator. In the same way, the total displacement at the top of a building (simulated total displacement) is obtained as the sum of the displacement at the bottom and the simulated relative displacement (drift) calculated by the Z-transform (Scaini et al., 2021). PSRD is calculated as the maximum of the relative displacement, i.e. the displacement between top and bottom. The displacement at the bottom is obtained by double integration of the recorded acceleration at the bottom. The recordings are band-pass filtered before integration. The cut off frequencies depend on the analyzed event (magnitude, distance, etc.) and the instruments recording the event (e.g., low cost sensors), and have to be defined for each test case to remove the part of the signal which is not related to the earthquake but to instrumental noise or is not of interest for the building's dynamic behavior. The interstory drift ratio can be obtained as the relative displacement divided by the building's height (Megalooikonomou et al., 2018). However, in this case, an average interstory drift is obtained, because the interstory drift is not linearly distributed over the different floors.

Damage assessment based on relative displacement or interstory drift limits

Expected damage is assessed by comparing the PSRD at the top of a building or the average interstory drift (calculated assuming

Figure 1. Photos of the buildings considered in this study: (a) Aviano, (b) Cividale, (c) Fogliano, (d) Gemona, (e) Gorizia, (f) Ronchi dei Legionari, (g) Tarvisio, (h) Tolmezzo and Visso (central Italy, panels i and j, respectively, for front and back view), and examples of installations at the bottom and top of the Aviano building (panels k and l, respectively). All photos with the exception of (i) and (j) are extracted from the Armonia project internal documentation. (i,j) The images of Visso school are extracted from the Osservatorio Sismico delle Strutture (OSS) documentation. The color version of this figure is available only in the electronic edition.

a constant floor height) with the limits provided in the literature for the considered building typology. If the thresholds are exceeded, extensive or complete damage is expected.

Studied Buildings—Input Parameters

In this study, we selected nine buildings (Fig. 1a–j) where earthquakes have been recorded by stations of the SMINO or OSS networks. The locations of the selected buildings and the epicenters of the recorded earthquakes are shown in Figure 2.

Eight buildings are located in northeastern Italy and are part of the SMINO network. These buildings were instrumented between 2018 and 2020, and have not suffered any damage until now (January 2023). In addition, a two-story simple stone URM school in Visso (central Italy), where the 2016 Central Italy sequence has been recorded, was studied. The Visso school building was part of the OSS and has been monitored by several sensors installed on each floor (e.g., Graziotti *et al.*, 2019; Lorenzoni *et al.*, 2019; Brunelli *et al.*, 2021). The school was severely damaged by the 24 August 2016 M_w 6.0 event (included in the data set) and has suffered further damage from the following events of the sequence. These events are not considered, because the estimation of cumulative damage is outside the scope of this study.

Building typology

The buildings (Fig. 1a–j), which are nowadays public, but some of them had residential use in the past, include examples of common building typologies in Italy, constructed of URM or RC, which are the most common materials (Table 2). In

absence of additional information on the URM type (Table 2), we assume that the buildings constructed before 1919 are simple stone masonry buildings. Ronchi Dei Legionari, where no information is available on the age of construction or masonry type, is conservatively considered a simple stone masonry building. Consequently, all masonry buildings are assumed to be simple stone URM buildings. Most of the studied RC buildings (Table 2) were constructed prior to the adoption of modern building codes. In Europe, except for some early examples of seismic codes (e.g., the 1915 regulations for Italy), the first building codes that account for seismic actions were introduced in the 1970s. This activity culminated in the late 1990s (Crowley *et al.*, 2021) when the first Eurocode was issued in 1998. In Italy, the National building code of 1996 already accounted for some of the principles included in the Eurocode. However, only a low fraction of buildings have been
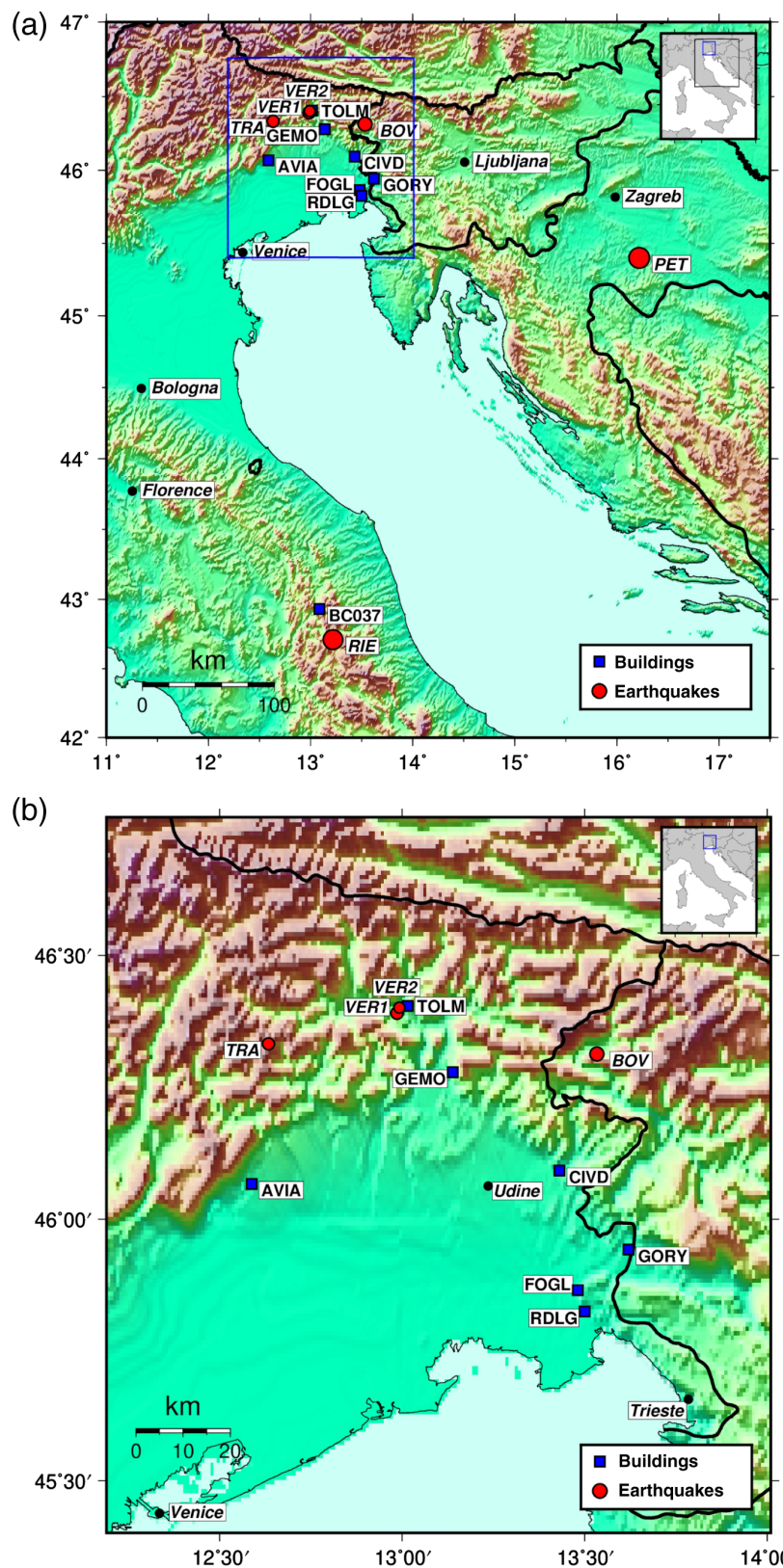
Figure 2. (a) Map with the locations of the epicenters of all studied earthquakes (red circles) and buildings (blue squares). The inset figure (in gray) shows the location of the studied area. The blue rectangle indicates the area shown in panel (b). (b) Map with location of earthquake epicenters and instrumented buildings in northeastern Italy. The color version of this figure is available only in the electronic edition.

retrofitted or renovated in the last few decades. Thus, the corresponding typologies are selected, assuming that RC frames are not seismically designed. Only the building in Tarvisio is a seismically designed shear-wall building, assuming a moderate ductility class in the corresponding seismic area. All the buildings have rigid floors, and their height is low- (1–2 stories) or mid-rise (3–5 stories). The selected buildings have different characteristics, such as footprint shape (regular or irregular) or year of construction. Many buildings are composed of multiple units (often due to the progressive enlargement of the building), and some of them are attached to other buildings. Building units are classified as regular or irregular (Table 2) based on their footprint shape. However, the buildings' regularity depends also on other factors, such as height (e.g., in presence of setbacks) and stiffness distribution (e.g., EC8, CEN, 2004). In addition, there are also some regular units that are attached to other units or to geotechnical structures (e.g., retention walls).

Vibration frequencies and oscillator type

The fundamental frequencies of the buildings used to initialize the SDOF or MDOF model (Table 2, x and y directions refer to the two main building axes) vary between 4 and 9 Hz. For the buildings of the SMINO network, the fundamental frequencies were estimated using ambient vibration recordings at different positions within the buildings using the spectral ratio method. This activity has

TABLE 2

Characteristics of the Considered Buildings and the Type of Oscillators (Single-Degree-of-Freedom [SDOF] or Multi-Degrees-of-Freedom [MDOF]) Used for the Analysis

Building ID	Building Location	Multiple Units	Standalone (S)/ Attached (A)	Structural Material	Construction Age	Retrofitted or Renovated	Height (m)	Floors Number	Shape of the Building Unit	SDOF or MDOF	f_i1 (Hz)	f_i2 (Hz)	Damping Ratio (%)	Instrumentation Year	First Evidence of Damage	Building Typology
AVIA	Aviano	Y	A	RC	>1976	Y	14	3	Regular	X: SDOF Y: SDOF	6.7 7.6		X: 10 Y: 5	2018	ND	Low-rise RC frame
CIVD	Cividale	Y	A	RC	1946–1960	N	12	3	Irregular	X: MDOF Y: MDOF	5.8 5.8	6.9 6.4	X: 3 Y: 3	2019	ND	Low-rise RC frame
FOGL	Fogliano	N	S	URM	<1919	Y	11	2	Irregular	X: MDOF Y: SDOF	7.2 6.7	8.2	X: 5 Y: 5	2019	ND	Low-rise simple stone URM
GEMO	Gemona	N	A	RC	>1976	N	12	3	Regular	X: MDOF Y: SDOF	7.0 6.4	10.8	X: 2 Y: 5	2019	ND	Low-rise RC frame
GORY	Gorizia	N	A	URM	<1919	Y	20	5	Irregular	X: MDOF Y: SDOF	3.5 4.6	3.8	X: 2 Y: 2	2019	ND	Mid-rise simple stone URM
RDLG	Ronchi dei Legionari	Y	A	URM	n.a.	N	11	4	Regular	X: SDOF Y: SDOF	6.3 5.7		X: 3 Y: 3	2019	ND	Mid-rise simple stone URM
TRVS	Tarvisio	Y	A	RC	2013	N	12	4	Regular	X: SDOF Y: SDOF	7.6 9.7		X: 5 Y: 5	2019	ND	Mid-rise RC shear walls
TOLM	Tolmezzo	N	A	URM	<1919	Y	11	4	Regular	X: SDOF Y: SDOF	6.3 5.7		X: 3 Y: 5	2018	ND	Mid-rise simple stone URM
BC037	Visso	N	S	URM	1930	N	13.4	2	Irregular (T shape)	X: SDOF Y: SDOF	4.1 3.2	15	X: 15 Y: 15	2012	August 2016	Low-rise simple stone URM

Many of the buildings have multiple units (column 3) or are attached to other buildings (column 4). The parameters in columns 5–17 refer to the building unit in which the sensors were installed (RC, reinforced concrete; and URM, unreinforced masonry). All sensors, with the exception of those installed in Visso, are low-cost accelerometers equipped with MEMS inertial sensors. ND, no damage observed; R, rectangular; S, square; and T, T-shape. f_i1 and f_i2 refer to the first and second vibration frequency (if applicable), respectively. i = x, y, i.e., the main building axes.

TABLE 3
Earthquakes for Which Ground-Motion Recordings are Available in the Selected Buildings (Table 2)

Event ID	Date (yyyy/mm/dd)	Location	Longitude, Latitude of Epicenter (°)	Magnitude	Distance Between Building and Epicenter (km)	Recorded in Building	Considered Frequency Range (Hz)
APP	2012/12/05	Appignano del Tronto, Italy	13.6600, 42.9100	M_L 4.0	47	BC037	0.5–40
ACC	2016/08/24	Accumoli, Italy	13.2200, 42.7100	M_W 6.0	26	BC037	0.2–40
VER1	2019/06/14	Verzegnis, Italy	12.9860, 46.3910	M_L 3.9	46	CIVD	1–12
					17	GEMO	1–12
					3	TOLM	1–12
VER2	2019/06/15	Verzegnis, Italy	12.9923, 46,4013	M_L 3.4	2	TOLM	1–12
TRA	2020/07/13	Tramonti di Sopra, Italy	12.6338, 46.3328	M_L 3.7	30	AVIA	1–12
BOV	2020/07/17	Bovec, Slovenia	13.5337, 46.3137	M_L 4.3	26	CIVD	1–12
					50	FOGL	1–12
					31	GEMO	1–12
					41	GORY	1–12
					41	TOLM	1–12
PET	2020/12/29	Petrinja, Croatia	16.2187, 45.4002	M_L 6.4	293	AVIA	2–12
					230	CIVD	1.5–12
					220	FOGL	1–12
					220	GORY	1–12
					218	RDLG	1–12
ZUG	2021/10/21	Zuglio, Italy	13.0797, 46.4286	M_L 3.8	39	TRVS	1–12
					6	TOLM	1–12

been carried out during the Armonia project (real-time acceleration network for monitoring sites and buildings in Italy and Austria, 2014–2020 INTERREG V-A Italy–Austria). The fundamental frequencies of the Visso school were taken from Ferrero et al. (2020); the two translational modes in x and y directions are considered. For the school in Visso, based on the available information, the SDOF oscillator simulation was carried out.

Damping ratio

The estimated damping ratio varies between 2% and 15% for the studied buildings (Table 2). The damping ratios are those obtained from a best-fit method using the recordings at the top of the building of the smallest considered event. The performance of the oscillators was tested by calculating the relative and total displacements and accelerations.

Damage thresholds

Table 1 shows the relative displacement limits for two damage levels (extensive and complete) for the considered building typologies (URM, consisting of stone or regular masonry and nonductile RC frames or moderate-ductility shear walls structures). Damage levels for both URM and RC buildings are defined based on the EMS-98 macroseismic scale (Grünthal, 1998). Relative displacement limits were estimated by Lagomarsino and Giovinazzi (2006) for European building typologies such as simple stone URM and RC buildings (frames or shear walls), which correspond to the M3, RC1, and RC2 types of the Lagomarsino and Giovinazzi (2006) classification. Moreover, the interstory drift limits are provided by Borzi et al. (2008) for URM and by the deliverables of the Risk-UE project (Mouroux and Brun, 2006) for RC. We associated the considered buildings with the corresponding building typologies.

The input parameters defining the oscillators (frequencies, damping, and SDOF or MDOF oscillator) and the damage thresholds have been set for each building using recordings of ambient vibration and a small-magnitude event, and are used for all the subsequent earthquakes.

Dataset of Ground-Motion Recordings

The characteristics of the considered events (Fig. 2), such as magnitude, location, and epicentral distance from the buildings where the events were recorded, are summarized in Table 3. All the recordings have been analyzed to determine the cutoff frequencies (Table 3) for each building–event pair and to remove instrumental noise or the part of the signal that is not of interest for estimating the building's dynamic behavior. All the sensors, except those installed in Visso (which belongs to the Italian OSS), are triaxial low-cost accelerometers equipped with micro electro-mechanical system inertial sensors. The low-cost sensors of the SMINO network were calibrated following the procedure described in Diez *et al.* (2006), originally defined for short-period seismometers. Their performance was then compared with that of conventional sensors, showing satisfactory results.

Results

The relative and total displacements at the top of each of the studied buildings (Table 2) were calculated for different seismic inputs (magnitudes, distances, and frequency contents) using DARR and the estimated parameters defining the oscillator (vibration frequencies, damping, and oscillator type). In the following, the estimation of the relative and total displacement at the top is shown and discussed in more detail for two selected buildings in northeastern Italy: a simple stone URM (Table 2, FOGL) and an RC building (Table 2, CIVD). The calculation was carried out for two events each: a local event of small magnitude (Table 3, BOV for FOGL and VER1 for CIVD) and the M_L 6.4 Petrinja, Croatia (Table 3, PET). Moreover, for the building BC037 in Visso (Table 2), the estimation of the relative and total displacements is presented for an M_L 4.0 (Table 3, APP) and the 24 August 2016 M_w 6.0 Central Italy events (Table 3, ACC). The FOGL building was modeled as an MDOF in the x direction and an SDOF oscillator in the y direction, whereas the CIVD building was modeled as an MDOF oscillator in both the directions. The dynamic behavior of BC037 building was simulated by SDOF oscillators in both the directions, using information on the fundamental frequencies from the literature (Ferrero *et al.*, 2020). All the three buildings shown here have an irregular footprint. Figure 3a,b,e,f shows the estimation of the relative and total displacements, and the Figure 3c,d,g,h corresponding displacement amplitude spectra for the FOGL building. Results are shown for the two main horizontal directions (x and y) of the FOGL building for two events: Figure 3a,b,c,d BOV and Figure 3e,f,g,h PET. In particular, from bottom to top are presented: (1) observed displacement at the bottom of the building (obtained by double integration of the recorded acceleration), (2) observed relative displacement at the top (obtained as difference of observed displacement at top and bottom), (3) simulated relative displacement at the top (calculated using Z-transform from the recording at

the bottom, e.g., Jin *et al.*, 2004), (4) simulated total displacement at the top of the building (determined as the sum of the simulated relative displacement and the displacement at the bottom), and (5) observed total displacement at the top (obtained by double integration of the recorded acceleration at the top of the building). Because low-cost sensors with a low sensitivity are installed in FOGL, for the BOV event, the signal below 1 Hz were related to instrumental noise. The response of the installed low-cost sensors is reliable in the range of frequencies between 0.2 and 12 Hz. For the reasons mentioned earlier, the recordings were filtered between 1 and 12 Hz for FOGL and BOV, respectively. For the PET event, the signals below 1 Hz are not related to instrumental noise but to low-frequency content of the earthquake itself. A comparison of the recordings of low-cost and conventional sensors was carried out. However, because FOGL has fundamental frequencies much higher than 1 Hz, and considering that the relative displacement is expected to be dominated by them, a 1–12 Hz band-pass filter was applied to the recordings.

FOGL is a standalone, single unit, and irregular simple stone URM building. The building's dynamic behavior is simulated in the x direction as an MDOF and in the y direction as an SDOF oscillator. The testing and definition of the model are carried out using the recordings of the BOV event and using the information on the modes obtained from the spectral ratios of ambient vibration measurements. The simulated and observed relative and total displacements at the top of the building are very similar, with a cross-correlation coefficient of 0.8 (FOGL and BOV, Fig. 3a,b) and 0.9–1 (FOGL and PET, Fig. 3c,d) for the total displacements. The differences between the relative displacements are slightly larger regarding the exact reconstruction of the traces. However, this is beyond the scope of our study that focuses on a first-order estimation of the expected damage to a built structure for rapid response purposes. For FOGL and BOV, there is a 10% difference between the simulated and observed PSRD—the parameter of interest for damage detection. The contribution of the relative to the total displacement at the top is significant for FOGL and BOV (Fig. 3a,b), whereas the total displacement at the top is almost equal to the displacement at the bottom of the building for FOGL and PET (Fig. 3e,f). This is due to the different frequency contents of the main energy contributions of the considered earthquakes (Fig. 3c,d,g,h; and Figs. S1 and S2, available in the supplemental material to this article). Although the energy contribution for FOGL and PET is in a frequency range up to 6 Hz, with the main contribution at about 2 Hz, the main vibrational modes of FOGL are at 7.2 and 8.2 Hz for the x and 6.7 Hz for the y direction. For BOV, the main energy content of the earthquake signal is in the same frequency range as the considered vibrational modes of the FOGL building. For both the events, the simulated PSRD (0.5 µm for FOGL and BOV and 0.1 mm for FOGL
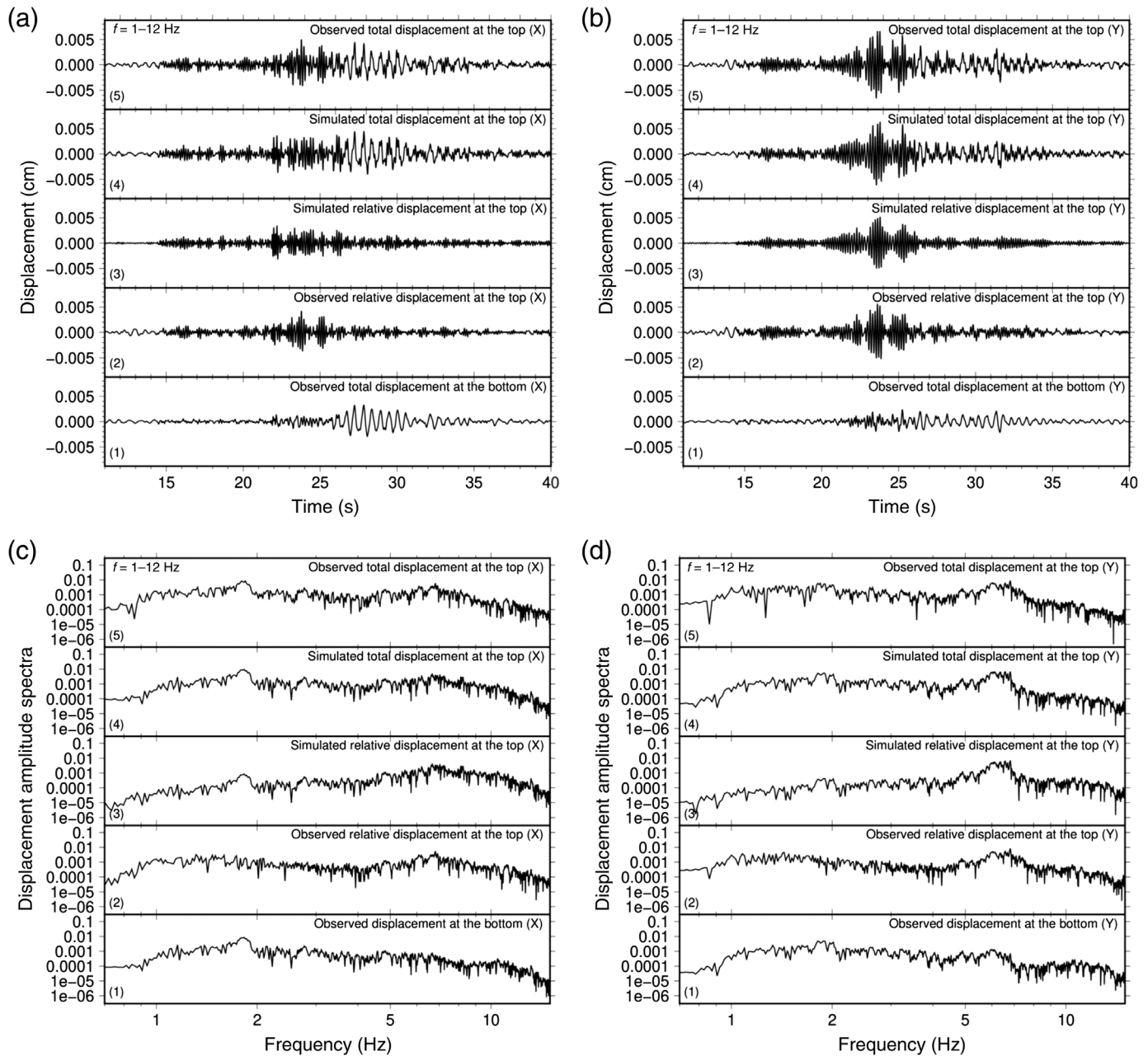
Figure 3. Estimation of the *x* (a,e) and *y* displacements (b,f) at the top of the FOGL building and the corresponding displacement spectral amplitude (*x*: c,g and *y*: d,h) for two selected events: (a,b, c,d) BOV and (e,f,g,h) PET. From bottom to top: (1) observed displacement at the bottom of a building (obtained by double integration of the recorded acceleration), (2) observed relative displacement at the top (obtained as difference of observed displacement at top and bottom), (3) simulated relative displacement at the top (calculated using Z-transform from the recording at the bottom), (4) simulated total displacement at the top of the building (determined as the sum of the drift and the displacement at the bottom), and (5) observed total displacement at the top (obtained by double integration of the recorded acceleration at the top of the building). Please note that different scales are used for subplots showing total or relative displacements for panel (e,f). (*Continued*)

and PET) are below the thresholds at which damage is expected (Table 1). Damage is also not expected when considering the interstory drift limits. There is no evidence of damage caused by the considered events in the building, which is currently (January 2023) in use.

Figures 4 and 5 show the same panels as Figure 3 without the corresponding displacement amplitude spectra from bottom to top for the two horizontal directions of two buildings (CIVD and BC037) for two different events each. Figure 4a,b presents the relative and total displacement estimates at the top for CIVD
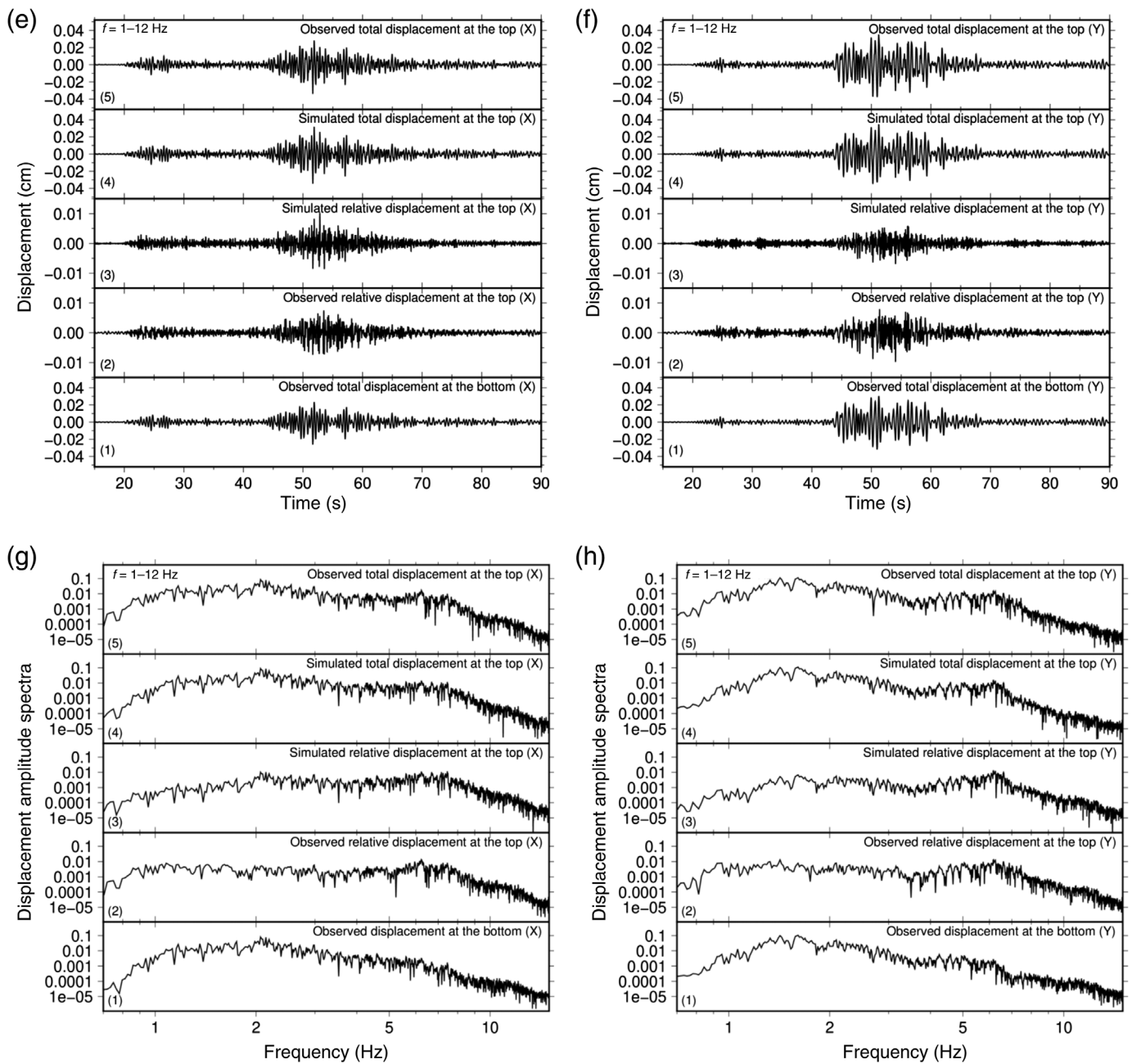
Figure 3. Continued

and VER1 and Figure 4c,d for CIVD and PET. CIVD is attached to other buildings and is composed of multiple units. The studied unit is constructed of reinforced concrete and has an irregular footprint. Because of the complex structure of the building and the information about the vibration modes obtained from the spectral ratios, the relative and total displacements at the top of the building were simulated with MDOF oscillators for both the horizontal directions of the building, giving satisfactory results. The differences between the simulated and recorded PSRD were up to 12% for CIVD and VER1 and about 15%

for CIVD and PET. The differences in the contribution of the drift to the total displacement at the top of the building for the two events can be explained in the same way as for the two events studied for FOGL (see Fig. 4 and Figs. S3 and S4). CIVD has not suffered any damage so far, the simulated PSRD for both the events (0.3 μm for CIVD and VER1 and 0.1 mm for CIVD and PET) are below the thresholds for which damage is expected (Table 1).

Figure 5 shows the results of the Visso school building (BC037, Table 2) for a small event in Figure 5b,c (APP,

Figure 4. Same as Figure 3a,b,e,f, without the corresponding displacement amplitude spectra. (a,b) CIVD and VER1 and (c, d) CIVD and PET. Please note that different scales are used for subplots showing total or relative displacements for panel (c,d).
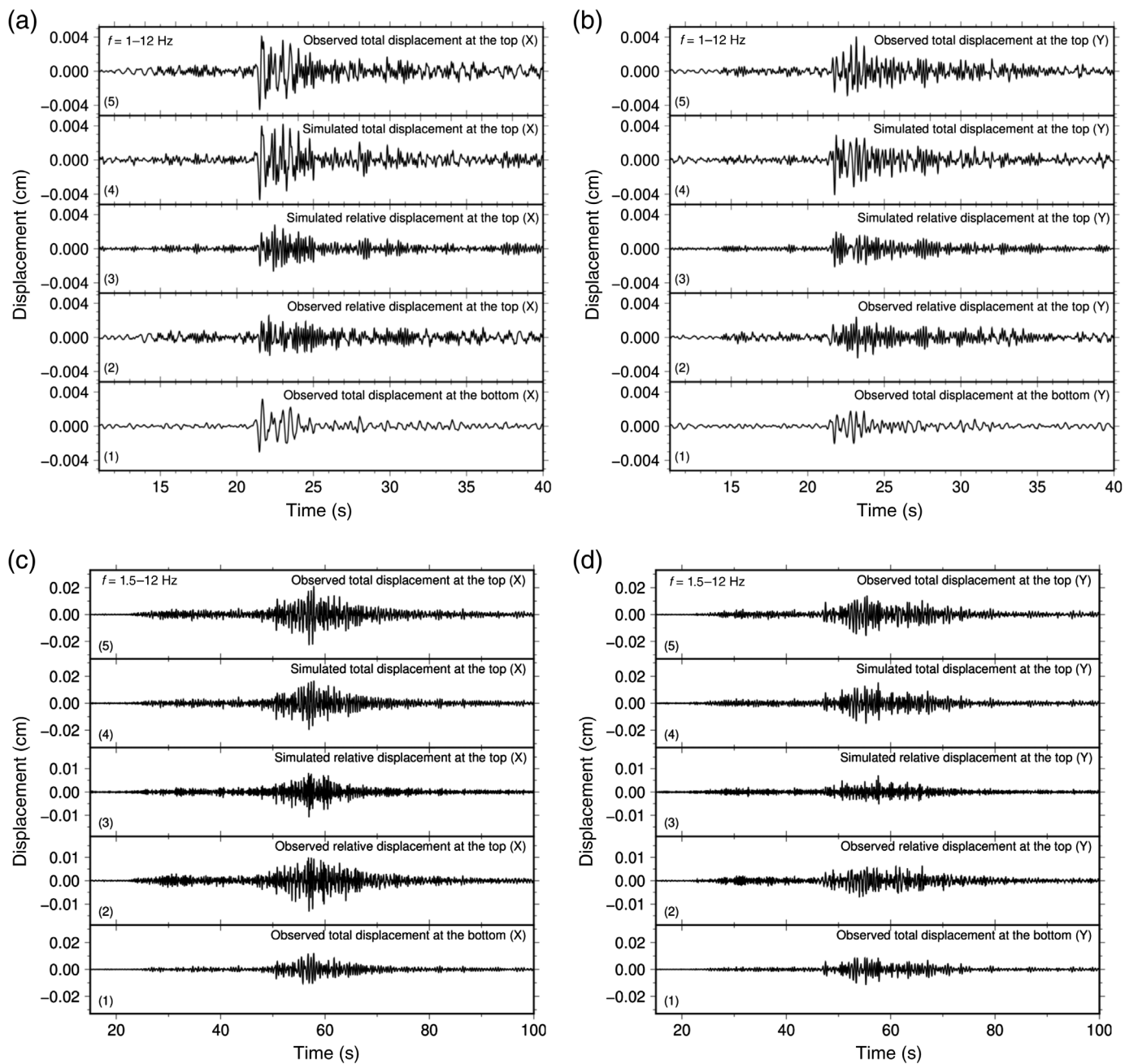
Table 3) and for the damaging M_w 6.0 event of 24 August 2016, in Figure 5d,e (ACC, Table 3). BC037 was a standalone simple stone URM building with a T-shape. Its dynamic behavior was simulated by SDOF oscillators in both the directions using values from the literature (e.g., Ferrero *et al.*, 2020). Differently from the buildings of the SMINO network, where one sensor is installed at the top and one at the bottom, four sensors were installed at the top of the Visso school building. In Figure 5b,c, d,e, we show the observed relative and total displacements for all the four sensors and their locations (Fig. 5a) with the same colors. Figures S5 and S6 show the observed accelerations, spectral amplitudes, and response spectra for APP and ACC, respectively. For both the events, the simulated and observed relative and total displacements at the top are similar, although

there is a discrepancy between the matching of the simulated and observed displacements. For the ACC event, there is a large variation of almost 50% between the observed relative displacements at the different points on the top, especially for the *y* direction. This is probably due to the irregular footprint of the building and the fact that the dynamic behavior of a T-shaped building is not the same at the different locations of the building. In addition, the building was damaged during this event.
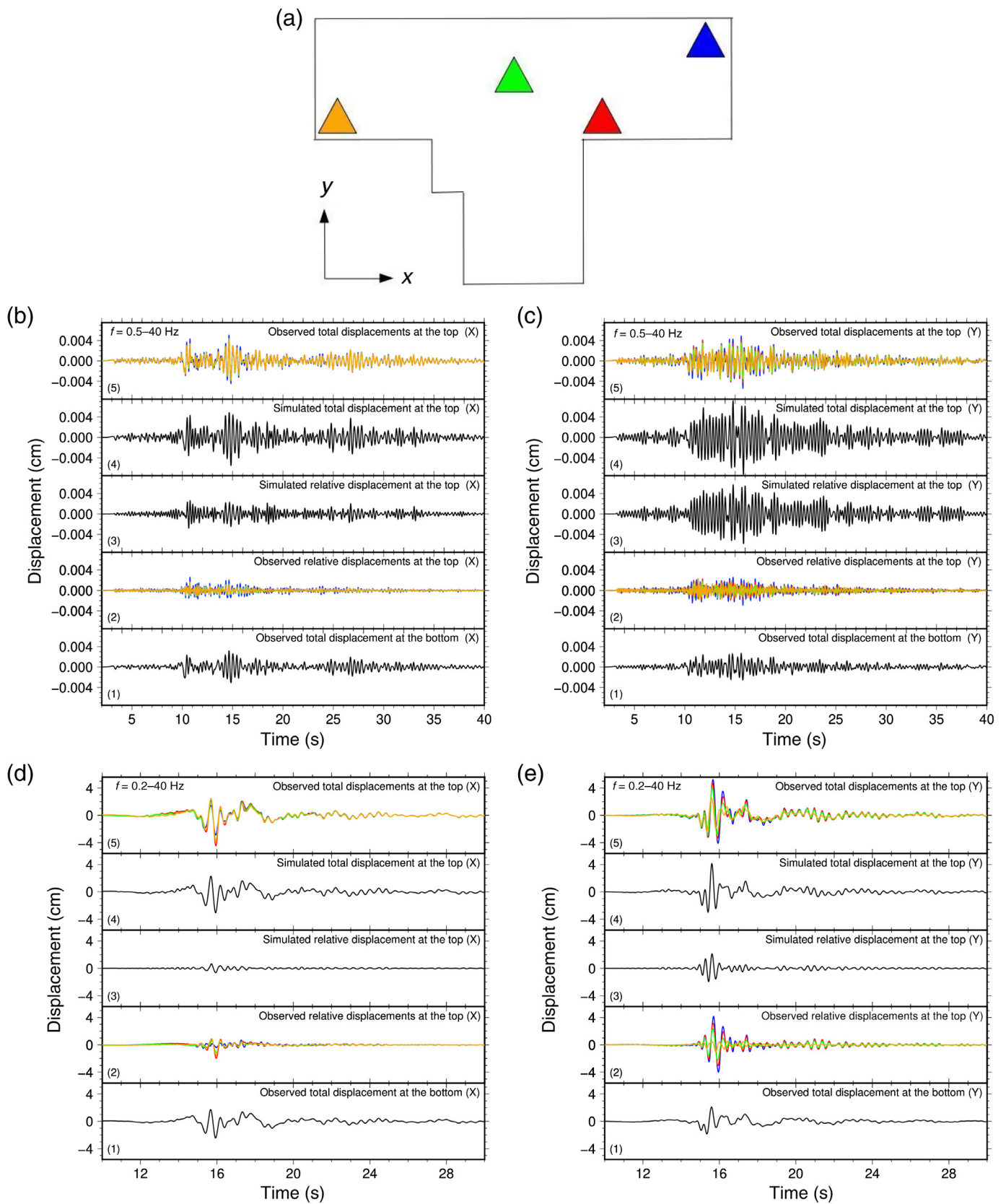
Figure 5. (a) Floor plan of the building showing the different locations of the sensors installed on the second floor. (b–e) Same as Figure 3a,b,e,f, without the corresponding displacement amplitude spectra: (b,c) BC037 and APP, and (d,e) BC037 and ACC. The different colors of the observed relative and total displacements correspond to the different locations of the sensors, as shown in the floor plan in panel (a). The color version of this figure is available only in the electronic edition.

13
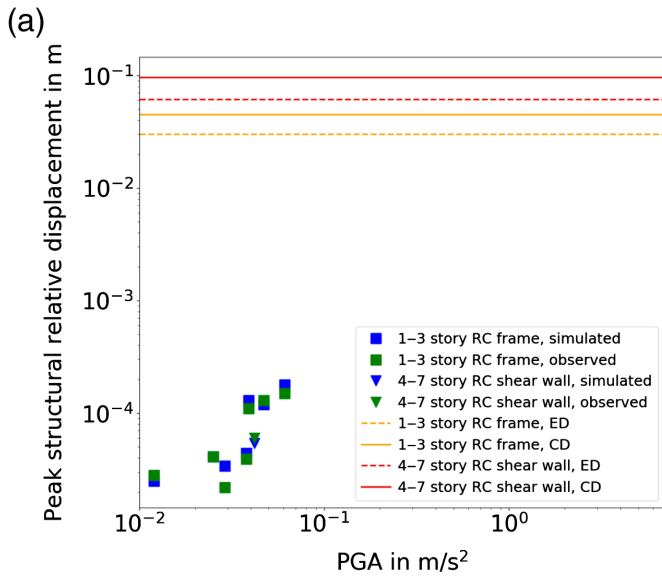
The simulated PSRD at the top of 0.6 μm for BC037 and APP is below the threshold for expected damage. This is consistent with the fact that the building has not been damaged by this event. For BC037 and ACC, the simulated PSRD was 2.1 cm, well above the threshold for complete damage for 1–2 story simple stone URM buildings (Table 1), in accordance with the fact that the building was severely damaged by the ACC event. However, the Visso school building with its 13.5 m was higher than an average two-story building. For this reason, the damage limits of 3–5 story simple stone URM buildings should be considered, resulting in extensive-complete damage.

Figure 6 summarizes the results of the considered events (Table 3) for all the selected buildings (Table 2). Figure 6a presents the results (blue indicates PSRD of simulated relative displacement, and green indicates PSRD of observed relative displacement) for the analyzed RC buildings (square indicates 1–3 story RC frame building, and triangle indicates 4–7 story RC shear-wall building) and the corresponding thresholds (Lagomarsino and Giovinazzi, 2006, Table 1) for extensive (ED, dashed lines) and complete damage (CD, solid lines). We calculated the PSRD for both the directions along the main building axes and took the maximum of the two values. The simulated and observed PSRD are, in general, very similar, although for some events the simulated PSRD is significantly higher or lower than the observed ones. All of the events recorded by the SMINO network were small, local, or larger distant events that resulted in PGAs below 0.1 m/s^2. In accordance with the information on the condition of the built structures, the PSRD for all RC building–event combinations is well below the thresholds at which damage is expected. Figure 6b shows the simulated (blue) and observed (green) PSRD for 1–2 story (squares) and 3–5 story (triangles) simple stone URM buildings and the corresponding thresholds for extensive (ED, dashed lines) and complete damage (CD, solid lines).
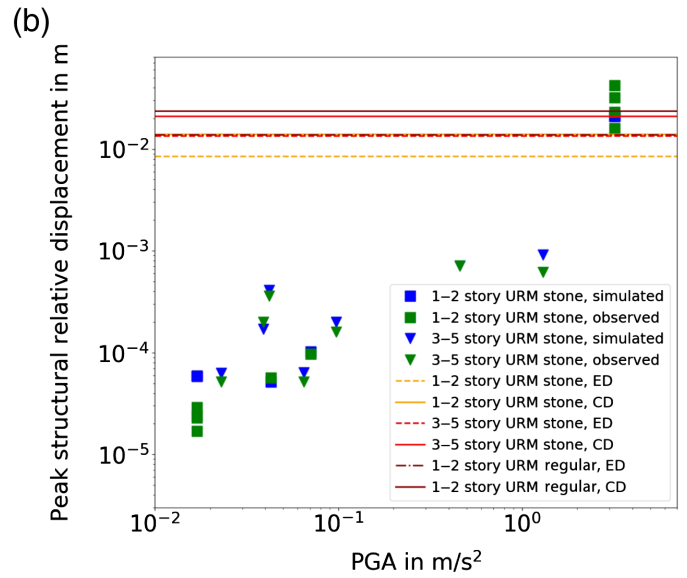
Figure 6. Comparison of simulated (blue) and observed peak structural relative displacement, PSRD (green) for all considered building-event combinations for (a) reinforced concrete (RC) and (b) simple stone unreinforced masonry (URM) buildings. The dashed or dashed-dotted and solid lines show the thresholds for different building typologies for extensive damage (ED) and complete damage (CD), respectively. The only building for which relative displacement thresholds were exceeded is the building BC037 in Visso during the ACC event (top-right corner). The color version of this figure is available only in the electronic edition.

Only for BC037 and ACC (shown in Fig. 5d,e), the PSRD exceeds the limits above which damage is expected. DARR successfully replicates the damage that occurred to the building under consideration. For all other URM building–event combinations, the simulated PSRD are below the thresholds and consistent with observations that no damage occurred.

Discussion

In this study, we applied DARR (proposed by Scaini et al., 2021) to analyze a set of different low- and mid-rise buildings (different materials, construction period, shape, composed of single or multiple units, attached, or standalone) under different seismic inputs (magnitude, epicentral distance, and frequency content). The selection of the buildings and events was limited by the low availability of recordings of the SMINO network on previously characterized low- and mid-rise buildings. In addition, no damaging event has been recorded in the vicinity. There are only a few buildings monitored by the OSS that have been damaged in the past. However, the other buildings (e.g., a school building in Norcia) have suffered cumulative damage that is outside the scope of our study.

DARR requires knowledge of the building typology, the choice of damage thresholds, and the characteristics of the

SDOF or MDOF oscillators adopted. For this reason, despite the simplicity of the method, a relatively rare combination of available seismological data and building characteristics is required. Its application should, therefore, be contemplated based on the availability and reliability of the required information. However, the available recordings allow testing if DARR simulates relative and total displacements satisfactorily for the selected buildings. DARR appears to be suitable for application to buildings located near the earthquake, where damage is expected to occur. The use of recordings from distant events (e.g., PET) allows to test the method, but raises problems in the choice of filter frequency, yet providing acceptable results in terms of PSRD.

The DARR method relies on a number of assumptions about the simplified building response, based on the linear behavior of an oscillator characterized by a certain damping ratio and fundamental frequency or frequencies. Under these assumptions, and in a first-order approximation, the building's dynamic behavior can be simulated by SDOF or MDOF oscillators. These oscillators simulate only the linear behavior of the structure, assuming that they can support the first-level identification of the occurrence of damage. The choice of the oscillator type is based on available information (fundamental frequencies from ambient noise measurements or the previous studies, and damping ratio). The performance of SDOF and MDOF was tested using available recordings. The parameters are estimated in advance from recordings of ambient vibration and a small-magnitude event, and used for all subsequent events. The choice of the model used may be different in the two directions (e.g., FOGL building). This is because the complexity of a building and, therefore, the dynamic behavior can be different in the two directions. In our study, the dynamic behavior of most of the buildings with a regular footprint was adequately simulated by SDOF oscillators, that of buildings with irregular footprint by MDOF oscillators. However, the selection of the oscillator type is not based on the footprint shape. Modeling buildings with irregular footprint by SDOF oscillators can give overall satisfactory results, as shown for BC037, for which information on the fundamental modes was limited to the first one. However, buildings with regular footprints may exhibit more complex dynamic behavior, when attached to other building units or geotechnical structures. In this case, MDOF oscillators are considered.

Prior analysis of the building is required to characterize the fundamental frequencies and damping (e.g., using ambient vibration recordings as in Gallipoli et al., 2009), and to test the performance of SDOF and MDOF with available earthquake recordings (preferably, but not necessarily more than one). In the absence of small-magnitude earthquake recordings and ambient noise measurements, period–height relationships for soil and building typologies (e.g., Gallipoli et al., 2020, 2023), and damping values from the literature (e.g., EC8, CEN, 2004) might be assumed, especially for simple buildings that can be modeled as SDOF oscillators. However, after the SDOF or MDOF parameters are defined for a specific building,

they are intended to be used for all further applications of DARR. As some examples show, the simulated total displacement was in reasonable agreement with the one obtained from measurements for the considered buildings and earthquake recordings. The exact reconstruction of the displacement time history is beyond the scope of this study, because PSRD is the parameter used for first-order rapid damage assessment. Figure 6 shows that the estimation of PSRD works well for most of the building–event combinations. However, for some building–event combinations, the PSRD was overestimated or underestimated. This may be due to the sensors used (e.g., low-cost versus conventional sensors), the signal processing, and the selected oscillator type (SDOF or MDOF) and its parameters (fundamental frequency and damping), or the fact that linear oscillators are used. In particular, the values of the damping ratio were estimated by selecting the best fitting values using the available earthquake recordings and testing some specific values from the literature. A more detailed study of the damping ratio could reduce the differences between the simulated and observed PSRD. Further, no distinction was made between rotational and translational modes, but rotational modes, when considered, were simulated in the same way as translational modes using SDOF or MDOF oscillators.

Finally, the building in Visso (BC037) was simulated with SDOF oscillators, using information about the fundamental modes from the literature. Considering also higher modes could improve the estimates of displacement and drift, this is especially true for small-magnitude events in which higher modes were excited, but were not considered in our study. For the damaging event, the PSRD is either overestimated or underestimated, depending on the considered observed relative displacement and the direction. The dynamic response of the Visso school is complex, and the observed relative and total displacements vary among the different measurement points (e.g., Ferrero et al., 2020). Simulating the dynamic behavior of a T-shaped building with an SDOF oscillator is an oversimplification, and, thus, the dynamic behavior of a T-shaped building is not exactly reproduced in all locations of the building by a single SDOF oscillator. Because only one recording is available at the bottom, we only obtain a relative and total displacement assumed for all locations at the top of the building. In addition, the underestimation or overestimation of the PSRD for the damaging event may be due to the fact that the parameters were selected for a linear dynamic behavior or to the selected damping ratio (15%). Moreover, the dynamic behavior may be different at different locations of the building due to the nonlinear behavior. For these reasons, the use of DARR might be associated with complementary damage estimates (e.g., based on fragility curves or recordings from conventional sensors). Nevertheless, the differences between the simulated and observed PSRD are small enough to allow a correct estimate of the expected damage. The simulated PSRD for the Visso school, which was extensively damaged by the ACC

earthquake (i.e., the first strong event of the seismic sequence), exceeded the thresholds for both the extensive and complete damage. This shows that the DARR method has the potential to identify the occurrence of structural damage for the considered building.

The contribution of relative displacement to total displacement varies for the different seismic inputs considered (magnitude, epicentral distance, and frequency content). As discussed previously, the contribution of the relative displacement depends on the frequency content of the main energy contribution of the earthquake and the frequency range of the vibrational modes of the studied building. Only if the considered vibrational modes are in the frequency range of the main energy content of the event, the drift will significantly contribute to the total displacement at the top of the building (e.g., Vanmarcke, 1976). In addition, other studies have observed low values of interstory drift in low-rise, stiff masonry buildings that suffered structural damage (Marino et al., 2016; Derakhshan and Griffith, 2018). For the analyzed buildings, the simulated interstory drift ratio (calculated as the average per height from the relative displacement) never exceeds the interstory drift limits, although damage has been observed for one building. The choice of thresholds may, therefore, vary between relative displacement and interstory drift, or a combination of both, depending on the characteristics of the selected building typology. The choice of thresholds should be pondered before applying the method and depends on the specific building typology considered. However, further research is needed to develop thresholds for both interstory drift and relative displacement for well-characterized building typologies, such as historical low-rise masonry buildings constructed with specific materials and/or techniques. In addition, thresholds should be associated with uncertainty levels obtained from analytical (Lagomarsino et al., 2020; Vaseghiamiri et al., 2020) or empirical (Martakis et al., 2022) analyzes to support a robust and conservative approach. Differently from the U.S. building codes (FEMA, 2012), European seismic codes do not provide relative displacement or interstory drift limits for structural damage. Relative displacement (drift) or interstory drift limits are usually derived using analytical models defined for common building typologies (e.g., Lagomarsino and Giovinazzi, 2006, for the most common European building typologies). For example, there are multiple damage thresholds associated with similar building typologies (e.g., different URM types, as in Table 1). According to Parolai et al. (2015), simulating a building's dynamic behavior using an SDOF oscillator is applicable to simple low-to-moderate-height structures for which dynamic response is dominated by the fundamental translational mode. Scaini et al. (2021) showed an application of the DARR method to simple, regular-in-shape buildings that are common in the studied area and in Italy. Petrovic et al. (2022) estimated the expected damage following the August 2016 M_w 6.0 Central Italy event for simple URM and RC buildings in different target areas using the DARR method. However, the building stock often includes complex buildings with different characteristics and of ambiguous interpretation (e.g., consisting of multiple attached units constructed at different times). In this study, despite the heterogeneity of the considered building types, the DARR method provided satisfactory results when applied to estimate the relative and total displacements at the top of low- and mid-rise buildings. The method reproduced relative and total displacements also for attached and irregular buildings. Moreover, it showed satisfactory results for earthquakes recorded at different distances and with different frequency contents.

The fundamental frequency and damping of the SDOF or MDOF used to model the buildings were estimated based on ambient vibration and small earthquakes recordings or taken from the literature. If recordings are not available, SDOF oscillators can be defined based on period–height relationships derived experimentally for specific building typologies (e.g., Scaini et al., 2021 for low-rise regular URM). In addition, the different soil conditions should be taken into account, as suggested by Gallipoli et al. (2023). However, the estimates might be refined using an MDOF oscillator. Using standard values for the damping ratio (e.g., 5% from EC8, CEN, 2004) could overestimate or underestimate the relative displacement for buildings with higher or lower damping ratios, respectively. However, when DARR is applied to building typologies (i.e., large sets of buildings) rather than specific buildings, an average damping value can be assumed to be representative.

In case the Visso school building was not a simple stone URM but a regular URM building, the simulated PSRD would still be well above the threshold above which extensive damage is expected for 1–2 story URM buildings. Thus, when assessing near-real-time expected damage, the adoption of the lower available threshold can provide reliable and conservative results even for ambiguous building typologies (e.g., unknown URM).

Here, we have shown that simplified building models can be applied and successfully reconstruct the peak structural relative displacement at the top for the buildings studied. Results are provided for a selected number of buildings with specific characteristics (low- and mid-rise URM and RC) and associated frequency range of main vibration modes (3–10 Hz) and for the available earthquake recordings. Further studies are needed to evaluate the validity of DARR for other building typologies characterized by different fundamental frequency ranges, stiffness, and damping. In addition, the PGA of the recordings used here are all below 0.1 m/s^2, with the exception of the recording in Visso which reaches 320 cm/s^2. Further analysis should be performed for other ground-motion levels (e.g., with larger PGA). DARR could potentially be applied to building typologies with similar characteristics, which are found at global, regional, and national scales (e.g., Jaiswal and Wald, 2008; Lang et al., 2018; Polese et al., 2019). However, its generalization should be carefully tested and validated for different building types, in particular, for those characterized by high ductility and/or strong

nonlinear behavior. In addition, DARR is intended only for the purpose of near-real-time damage assessment, and its use should be complemented by more sophisticated analyzes to assess the damage state and structural health of the building.

The method presented here underlines the importance of cost-effective building monitoring networks installed in urban areas. Different earthquake recordings for monitored buildings allow better characterization of the oscillators used for DARR and help increase the spatial resolution of damage assessment compared to traditional methods (e.g., Silva and Horspool, 2019; Dolce *et al.*, 2021; Poggi *et al.*, 2021).

Conclusions

In this study, we tested the DARR method proposed by Scaini *et al.* (2021), which estimates the peak structural relative displacement at the top of a building from a recording at the ground as well as the expected damage state based on predefined thresholds. DARR can be applied under certain assumptions that simplify the dynamic behavior of low- and mid-rise buildings; but it needs to be tested for other building types. We have shown that DARR can reproduce the simplified dynamic behavior of the selected buildings, and, in particular, the relative and total displacement at the top in a first approximation. This is true for a set of considered ground-motion recordings (19) and for the analyzed building types (a total of nine low- and mid-rise buildings). The results show that based on a single earthquake recording, it is possible to estimate the peak structural relative displacement in the previously characterized buildings. This supports the assessment of expected damage for buildings for which a set of parameters, including fundamental frequency and damping, are known. Our analyses have shown that for events of moderate-to-high-magnitude recorded near the buildings, noise from low-cost sensors does not affect the signal quality. Thus, low-cost sensors can support the application of DARR for the purpose of rapid damage estimates. In addition, DARR can potentially be extended to buildings in an area surrounding the earthquake recording (target area), as long as they belong to the previously characterized typologies for which the method has proven validity. It can, therefore, likely support the estimation of first-level damage of the building stock based on earthquake recordings in seismically active areas with seismic monitoring networks in place.

Data and Resources

The recordings at the Visso building were obtained from the Italian structural seismic monitoring network (Dolce *et al.*, 2017) and are available upon registration available at https://oss.protezionecivile.it/osspublic/#/ (last accessed December 2021). The supplemental material includes the observed accelerations, the spectral amplitudes, and the response spectra for the building–event pairs shown in Figures 3–5.

Declaration of Competing Interests

The authors acknowledge that there are no conflicts of interest recorded.

References

Bindi, D., I. Iervolino, and S. Parolai (2016). On-site structure-specific real-time risk assessment: Perspectives from the REAKT project, *Bull. Earthq. Eng.* **14,** 2471–2493, doi: 10.1007/s10518-016-9889-4.

Bindi, D., B. Petrovic, S. Karapetrou, M. Manakou, T. Boxberger, D. Raptakis, K. D. Pitilakis, and S. Parolai (2015). Seismic response of an 8-story RC-building from ambient vibration analysis, *Bull. Earthq. Eng.* **13,** 2095–2120, doi: 10.1007/s10518-014-9713-y.

Borzi, B., H. Crowley, and R. Pinho (2008). Simplified pushover-based earthquake loss assessment (SP-BELA) method for masonry buildings, *Int. J. Arch. Herit.* **2,** no. 4, 353–376.

Bragato, P. L., P. Comelli, A. Saraò, D. Zuliani, L. Moratto, V. Poggi, G. Rossi, C. Scaini, M. Sugan, C. Barnaba, *et al.* (2021). The OGS—Northeastern Italy seismic and deformation network: Current status and outlook, *Seismol. Res. Lett.* **92,** no. 3, 1704–1716, doi: 10.1785/0220200372.

Brunelli, A., F. de Silva, A. Piro, F. Parisi, S. Sica, F. Silvestri, and S. Cattari (2021). Numerical simulation of the seismic response and soil–structure interaction for a monitored masonry school building damaged by the 2016 Central Italy earthquake, *Bull. Earthq. Eng.* **19,** 1181–1211, doi: 10.1007/s10518-020-00980-3.

CEN (2004). *European Standard EN 1998-1: 2005 Eurocode 8: Design of Structures for Earthquake Resistance. Part 1: General Rules, Seismic Action and Rules for Buildings*, European Committee for Standardization, Brussels, Belgium.

Chourasia, A., S. K. Bhattacharyya, N. M. Bhandari, and P. Bhargava (2016). Seismic performance of different masonry buildings: Full-scale experimental study, *J. Perform. Constr. Facil.* **30,** no. 5, 2016, doi: 10.1061/(ASCE)CF.1943-5509.0000850.

Clayton, R. W., T. Heaton, M. Chandy, A. Krause, M. Kohler, J. Bunn, R. Guy, M. Olson, M. Faulkner, M. Cheng, *et al.* (2012). Community seismic network, *Ann. Geophys.* **54,** no. 6, doi: 10.4401/ag-5269.

Crowley, H., V. Despotaki, D. Rodrigues, V. Silva, D. Toma-Danila, E. Riga, A. Karatzetzou, S. Fotopolou, Z. Zugic, L. Sousa, *et al.* (2020). Exposure model for European seismic risk assessment, *Earthq. Spectra* **36,** 252–273, doi: 10.1177/8755293020919429.

Crowley, H., V. Despotaki, V. Silva, J. Dabbeek, X. Romão, N. Pereira, J. M. Castro, J. Daniell, E. Veliu, H. Bilgin, *et al.* (2021). Model of seismic design lateral force levels for the existing reinforced concrete European building stock, *Bull. Earthq. Eng.* **19,** 2839–2865, doi: 10.1007/s10518-021-01083-3.

Da Porto, F., M. Donà, A. Rosti, M. Rota, S. Lagomarsino, S. Cattari, B. Borzi, M. Onida, D. De Gregorio, F. L. Perrelli, *et al.* (2021). Comparative analysis of the fragility curves for Italian residential

masonry and RC buildings, *Bull. Earthq. Eng.* **19,** 3209–3252, doi: 10.1007/s10518-021-01120-1.

Derakhshan, H., and M. Griffith (2018). *Final Rept. on Pushover Analysis of Classes of Unreinforced Masonry Buildings to Characterise Drift Ratios for Different Damage Levels*, Bushfire and Natural Hazards CRC, Melbourne, available at https://www.bnhcrc.com.au/sites/default/files/managed/downloads/1.2.1._drift_damage.pdf (last accessed January 2023).

Diez, E., D. Zuliani, and F. Ponton (2006). Cuban seismic network short period seismometer calibration, *IC/IR/2006/006 Internal Rept. for "The Abdus Salam International Center for Theoretical Physics—ICTP"*, doi: 10.13140/RG.2.1.3825.0649.

Dolce, M., M. Nicoletti, A. De Sortis, S. Marchesini, D. Spina, and F. Talanas (2017). Osservatorio sismico delle strutture: The Italian structural seismic monitoring network, *Bull. Earthq. Eng.* **15,** 621–641, doi: 10.1007/s10518-015-9738-x.

Dolce, M., A. Prota, B. Borzi, F. Da Porto, S. Lagomarsino, G. Magenes, C. Moroni, A. Penna, M. Polese, E. Speranza, *et al.* (2021). Seismic risk assessment of residential buildings in Italy, *Bull. Earthq. Eng.* **19,** 2999–3032, doi: 10.1007/s10518-020-01009-5.

Donà, M., P. Carpanese, V. Follador, L. Sbrogiò, and F. Da Porto (2020). Mechanics-based fragility curves for Italian residential URM buildings, *Bull. Earthq. Eng.* doi: 10.1007/s10518-020-00928-7.

Ebrahimian, M., M. D. Trifunac, and M. I. Todorovska (2016). Prediction of building response at any level from recorded roof response: The Kanai–Yoshizawa formula revisited, *Soil Dynam. Earthq. Eng.* **80,** 241–250, doi: 10.1016/j.soildyn.2015.08.001.

Espinosa-Aranda, L. M., A. Cuellar, A. Garcia, G. Ibarrola, R. Islas, S. Maldonado, and F. H. Rodriguez (2009). Evolution of the Mexican seismic alert system (SASMEX), *Seismol. Res. Lett.* **80,** no. 5, 694–706, doi: 10.1785/gssrl.80.5.694.

Federal Emergency Management Agency (FEMA) P-58-1 (2012). *Seismic Performance Assessment of Buildings, Volume 1—Methodology*, Federal Emergency Management Agency, Washington, D.C.

Ferrero, C., P. B. Lourenco, and C. Calderini (2020). Nonlinear modeling of unreinforced masonry structures under seismic actions: Validation using a building hit by the 2016 Central Italy earthquake, *Frattura ed Integrità Strutturale* **14,** no. 51, 92–114, doi: 10.3221/IGF-ESIS.51.08.

Fiorentino, G., A. Forte, E. Pagano, F. Sabetta, C. Baggio, D. Lavorato, C. Nuti, and S. Santini (2018). Damage patterns in the town of Amatrice after August 24th 2016 Central Italy earthquakes, *Bull. Earthq. Eng.* **16,** 1399–1423, doi: 10.1007/s10518-017-0254-z.

Frankie, T. M., B. Gencturk, and A. S. Elnashai (2013). Simulation-based fragility relationships for unreinforced masonry buildings, *J. Struct. Eng.* **139,** 400–410, doi: 10.1061/(ASCE)ST.1943-541X.000064.

Gallipoli, M. R., G. Calamita, N. Tragni, D. Pisapia, M. Lupo, M. Mucciarelli, T. Stabile, A. Perrone, L. Amato, F. Izzi, *et al.* (2020). Evaluation of soil-building resonance effect in the urban area of the city of Matera (Italy), *Eng. Geol.* **272,** 105645, doi: 10.1016/j.eng-geo.2020.105645.

Gallipoli, M. R., M. Mucciarelli, and M. Vona (2009). Empirical estimate of fundamental frequencies and damping for Italian buildings, *Earthq. Eng. Struct. Dynam.* **38,** 973–988, doi: 10.1002/eqe.878.

Gallipoli, M. R., B. Petrovic, C. Scaini, G. Calamita, N. Tragni, C. Barnaba, M. Vona, and S. Parolai (2023). Towards specific T-H relationships: FRIBAS database for better characterization of RC and URM buildings, *Bull. Earthq. Eng.* doi: 10.1007/s10518-022-01594-7.

Gorini, A., M. Nicoletti, P. Marsan, R. Bianconi, R. NardisDe, L. Filippi, S. Marcucci, F. Palma, and E. Zambonelli (2010). The Italian strong motion network, *Bull. Earthq. Eng.* **8,** 1075–1090, doi: 10.1007/s10518-009-9141-6.

Graziotti, F., M. Solenghi, G. Guerrini, and A. Penna (2019). Macroelement modelling of a monitored URM school building accounting for seismic damage accumulation, *Proc. of the XVIII ANIDIS Conference*, Ascoli Piceno, Italy, 15–19 September 2019.

Grünthal, G. (1998). (Editor) European Macroseismic Scale 1998 (EMS-98), in *Cahiers du Centre Européen de Géodynamique et de Séismologie*, Vol. 15, Centre Européen de Géodynamique et de Séismologie, Luxembourg, 99 pp (in French).

Iervolino, I., M. Giorgio, and E. Chioccarelli (2016). Markovian modeling of seismic damage accumulation, *Earthq. Eng. Struct. Dyn.* **45,** no. 3, 441–461.

Jaiswal, K. S., and D. J. Wald (2008). Creating a global building inventory for earthquake loss assessment and risk management, *U.S. Geol. Surv. Open-File Rept. 2008-1160*, 106 pp.

Jin, X., Q. Ma, and S. Li (2004). Comparison of four numerical methods for calculating seismic dynamic response of SDOF systems, *13th World Conf. on Earthquake Engineering*, Vancouver, Canada, 1–6 August 2004.

Lagomarsino, S., and S. Giovinazzi (2006). Macroseismic and mechanical models for the vulnerability and damage assessment of current buildings, *Bull. Earthq. Eng.* **4,** 415–443, doi: 10.1007/s10518-006-9024-z.

Lagomarsino, S., S. Marino, and S. Cattari (2020). Linear static procedures for the seismic assessment of masonry buildings: Open issues in the new generation of European codes, *Structures* **26,** 427–440, doi: 10.1016/j.istruc.2020.04.003.

Lang, D. H., A. Kumar, S. Sulaymanov, and A. Meslem (2018). Building typology classification and earthquake vulnerability scale of Central and South Asian building stock, *J. Build. Eng.* **15,** 261–277, doi: 10.1016/j.jobe.2017.11.022.

Lee, V. W. (1990). Efficient algorithm for computing displacement, velocity and acceleration responses of an oscillator to arbitrary ground motion, *Soil Dynam. Earthq. Eng.* **l9,** no. 6, 288–300.

Lorenzoni, F., A. Calabria, N. De Conto, and F. Portoda (2019). Assessment of the dynamic response of monitored masonry buildings after the Central Italy earthquake swarm in 2016, *COMPDYN*, Crete, Greece, 24–26 June 2019.

Marino, S., S. Cattari, and S. Lagomarsino (2016). Modelling of two damaged unreinforced masonry buildings following the Canterbury earthquakes, *2016 NZSEE Conference*, 1–3 April 2016.

Martakis, P., Y. Reuland, M. Imesch, and E. Chatzi (2022). Reducing uncertainty in seismic assessment of multiple masonry buildings based on monitored demolitions, *Bull. Earthq. Eng.* **20,** 4441–4482, doi: 10.1007/s10518-022-01369-0.

Masi, A., L. Chiauzzi, G. Santarsiero, V. Manfredi, S. Biondi, E. Spacone, C. Del Gaudio, P. Ricci, G. Manfredi, and G. M. Verderame (2019). Seismic response of RC buildings during the Mw 6.0 August 24,

2016 Central Italy earthquake: The Amatrice case study, *Bull. Earthq. Eng.* **17,** 5631–5654, doi: 10.1007/s10518-017-0277-5.

Megalooikonomou, K. G., S. Parolai, and M. Pittore (2018). Toward performance-driven seismic risk monitoring for geothermal platforms: Development of ad hoc fragility curves, *Geotherm. Energy* **6,** doi: 10.1186/s40517-018-0094-3.

Mori, J., H. Kanamori, J. Davis, E. Hauksson, E. Clayton, T. Heaton, L. Jones, A. Shakal, and R. Porcella (1998). Major improvements in progress for southern California earthquake monitoring, *Eos Trans. AGU* **79,** 217–221.

Mouroux, P., and B. L. Brun (2006). Presentation of RISK-UE Project, *Bull. Earthq. Eng.* **4,** 323–339, doi: 10.1007/s10518-006-9020-3.

Mucciarelli, M., and M. R. Gallipoli (2007). Non-parametric analysis of a single seismometric recording to obtain building dynamic parameters, *Ann. Geophys.* **50,** no. 2, 259–266, doi: 10.4401/ag-3079.

Okada, Y., K. Kasahara, S. Hori, K. Obara, S. Sekiguchi, H. Fujiwara, and A. Yamamoto (2004). Recent progress of seismic observation networks in Japan—Hi-net, F-net, K-NET and KiK-net—, *Earth Planets Space* **56,** xv–xxviii, doi: 10.1186/BF03353076.

Parolai, S., D. Bindi, T. Boxberger, C. Milkereit, K. Fleming, and M. Pittore (2015). On-site early warning and rapid damage forecasting using single stations: Outcomes from the REAKT project, *Seismol. Res. Lett.* **86,** no. 5, 1393–1404, doi: 10.1785/0220140205.

Parolai, S., T. Boxberger, M. Pilz, K. Fleming, M. Haas, M. Pittore, B. Petrovic, B. Moldobekov, A. Zubovich, and J. Lauterjung (2017). Assessing earthquake early warning using sparse networks in developing countries: Case study of the Kyrgyz Republic, *Front. Earth Sci.* **5,** 74, doi: 10.3389/feart.2017.00074.

Petrovic, B., S. Parolai, G. Pianese, S. U. Dikmen, B. Moldobekov, S. Orunbaev, and R. Paolucci (2018). Joint deconvolution of building and downhole seismic recordings: An application to three test cases, *Bull. Earthq. Eng.* **16,** 613–641, doi: 10.1007/s10518-017-0215-6.

Petrovic, B., C. Scaini, and S. Parolai (2022). Applying the damage assessment for rapid response approach to the August 24 M 6 event of the seismic sequence in Central Italy (2016), *Front. Earth Sci.* **10,** doi: 10.3389/feart.2022.932110.

Picozzi, M., S. Parolai, M. Mucciarelli, C. Milkereit, D. Bindi, R. Ditommaso, M. Vona, M. R. Gallipoli, and J. Zschau (2011). Interferometric analysis of strong ground motion for structural health monitoring: The example of the L'Aquila, Italy, seismic sequence of 2009, *Bull. Seismol. Soc. Am.* **101,** no. 2, 635–651, doi: 10.1785/0120100070.

Poggi, V., C. Scaini, L. Moratto, G. Peressi, P. Comelli, P. L. Bragato, and S. Parolai (2021). Rapid damage scenario assessment for earthquake emergency management, *Seismol. Res. Lett.* **92,** no. 4, 2513–2530, doi: 10.1785/0220200245.

Polese, M., M. Gaetani, A. D'Aragona, and A. Prota (2019). Simplified approach for building inventory and seismic damage assessment at the territorial scale: An application for a town in southern Italy, *Soil Dynam. Earthq. Eng.* **121,** 405–420, doi: 10.1016/j.soildyn.2019.03.028.

Rahmani, M., and M. I. Todorovska (2021). Structural health monitoring of a 32-storey steel-frame building using 50 years of seismic monitoring data, *Earthq. Eng. Struct. Dynam.* **50,** 1777–1800, doi: 10.1002/eqe.3422.

Rahmani, M., M. Ebrahimian, and M. I. Todorovska (2015). Time-wave velocity analysis for early earthquake damage detection in buildings: Application to a damaged full-scale RC building, *Earthq. Eng. Struct. Dynam.* **44,** no. 4, 619–636.

Rossetto, T., P. Gehl, S. Minas, C. Galasso, P. Duffour, J. Douglas, and O. Cook (2016). FRACAS: A capacity spectrum approach for seismic fragility assessment including record-to-record variability, *Eng. Struct.* **125,** 337–348, doi: 10.1016/j.engstruct.2016.06.043.

Rota, M., A. Penna, and C. L. Strobbia (2008). Processing Italian damage data to derive typological fragility curves, *Soil Dynam. Earthq. Eng.* **28,** nos. 10/11, 933–947.

Ruiz-García, J., and M. Negrete (2009). A simplified drift-based assessment procedure for regular confined masonry buildings in seismic regions, *J. Earthq. Eng.* **13,** no. 4, 520–539, doi: 10.1080/13632460802598560.

Satriano, C., L. Elia, C. Martino, M. Lancieri, A. Zollo, and G. Iannaccone (2011). PRESTo, the earthquake early warning system for southern Italy: Concepts, capabilities and future perspectives, *Soil Dynam. Earthq. Eng.* **31,** 137–153, doi: 10.1016/j.soildyn.2010.06.008.

Scaini, C., B. Petrovic, A. Tamaro, L. Moratto, and S. Parolai (2021). Near-real-time damage estimation for buildings based on strong-motion recordings: An application to target areas in northeastern Italy, *Seismol. Res. Lett.* **92,** no. 6, 3785–3800, doi: 10.1785/0220200430.

Silva, V., and N. Horspool (2019). Combining USGS ShakeMaps and the OpenQuake-engine for damage and loss assessment, *Earthq. Eng. Struct. Dynam.* **48,** no. 6, 634–652, doi: 10.1002/eqe.3154.

Snieder, R., and E. Safak (2006). Extracting the building response using seismic interferometry: Theory and application to the Millikan library in Pasadena, California, *Bull. Seismol. Soc. Am.* **96,** no. 2, 586–598.

So, E., and R. Spence (2013). Estimating shaking-induced casualties and building damage for global earthquake events: A proposed modelling approach, *Bull. Earthq. Eng.* **11,** 347–363, doi: 10.1007/s10518-012-9373-8.

Straser, E. G., and A. S. Kiremidjian (1998). *A Modular, Wireless Damage Monitoring System for Structures, Rept. No. 128*, John A. Blume Earthquake Engineering Center, Stanford University, Stanford.

Trifunac, M. D., T. Y. Hao, and M. I. Todorovska (2001). Response of A 14-story reinforced concrete structure to nine earthquakes: 61 years of observation in the Hollywood storage building, *Report CE 01-02*, available at https://cpb-us-e1.wpmucdn.com/sites.usc.edu/dist/f/100/files/2018/03/R117CE_01_02-2j8v6hq.pdf (last accessed January 2023).

Vanmarcke, E. H. (1976). Structural response to earthquakes, in *Seismic Risk and Engineering Decisions*, C. Lomnitz and E. Rosenblueth (Editors), Vol. 15, Developments in Geotechnical Engineering, Elsevier Publishing Company, Amsterdam, The Netherlands, 278–337.

Vaseghiamiri, S., M. Mahsuli, M. A. Ghannad, and F. Zareian (2020). Surrogate SDOF models for probabilistic performance assessment of multistory buildings: Methodology and application for steel special moment frames, *Eng. Struct.* **212,** 110276, doi: 10.1016/j.engstruct.2020.110276.

Wald, D. J., P. S. Earle, T. I. Allen, K. Jaiswal, K. Porter, and M. Hearne (2008). Development of the U.S. Geological Survey's PAGER system (prompt assessment of global earthquakes for response), *Proc. of the 14th World Conf. on Earthquake Engineering*, Beijing, China, 12–17 October 2008, 8 pp.

Wald, D. J., P. S. Earle, K. W. Lin, V. Quitoriano, and B. C. Worden (2006). Challenges in rapid ground motion estimation for the prompt assessment of global urban earthquakes, *Bull. Earthq. Res. Inst.* **81,** 275–283.

Wald, D. J., V. Quitoriano, T. H. Heaton, H. Kanamori, C. W. Scrivner, and C. B. Worden (1999). TriNet "ShakeMaps": Rapid generation of peak ground motion and intensity maps for earthquakes in Southern California, *Earthq. Spectra* **15,** 537–555.

Wald, L. A., D. J. Wald, S. Schwarz, B. Presgrave, P. S. Earle, E. Martinez, and D. Oppenheimer (2008). The USGS earthquake notification service (ENS): Customizable notifications of earthquakes around the globe, *Seismol. Res. Lett.* **79,** no. 1, 103–110.

Wessel, P., J. F. Luis, L. Uieda, R. Scharroo, F. Wobbe, W. H. F. Smith, and D. Tian (2019). The generic mapping tools version 6, *Geochem. Geophys.* **20,** 5556–5564, doi: 10.1029/ 2019GC008515.

Wu, W. M., D.-Y. Chen, T.-L. Lin, C.-Y. Hsieh, T.-L. Chin, W.-Y. Chang, W.-S. Li, and S.-H. Ker (2013). A high- density seismic network for earthquake early warning in Taiwan based on low cost sensors, *Seismol. Res. Lett.* **84,** no. 6, 1048–1054, doi: 10.1785/ 0220130085.